Minerals Engineering 55 (2014) 80–86

Contents lists available at ScienceDirect

Minerals Engineering

journal homepage: www.elsevier.com/locate/mineng

Refinement of the isomorphic substitutions in goethite and hematite by the Rietveld method, and relevance to bauxite characterisation and processing

Reiner Neumann [a,*], Angela Nair Avelar [b], Geraldo Magela da Costa [c]

[a] CETEM – Centre for Mineral Technology, Division for Technological Characterisation, Avenida Pedro Calmon, 900, 21941-908 Rio de Janeiro, RJ, Brazil
[b] Vale SA, Process Development Americas, Santa Luzia, MG, Brazil
[c] Chemistry Department, Universidade Federal de Ouro Preto, Ouro Preto, MG, Brazil

ARTICLE INFO

Keywords:
Bauxite
X-ray diffraction
Rietveld method
Mineral phase quantification
Isomorphous substitution
Mixed crystals

ABSTRACT

Although bauxites usually have a quite simple mineralogy – gibbsite (+boehmite), quartz, kaolinite, hematite, goethite, anatase (+rutile) and minor or less common phases, fine particle size, low crystallinity and variable compositions of the iron minerals might render phase quantification difficult, as well as impairing bauxite processing. A reliable and complete characterisation is therefore necessary in order to predict processing performance and ensure compliance to plant specifications.

X-ray diffraction is the most important single tool for bauxite characterisation, and the constrained refinement of the Al-for-Fe substitution in goethite during one-step phase quantification by fundamental parameters Rietveld method has been successfully used. The same method was developed to analyse the coupled Al-for-Fe and OH^--for-O^{2-} substitutions in hematite. The method was tested against Mössbauer spectroscopy iron distribution on bauxite samples with a large compositional range, and on bauxite Certified Reference Materials from the main Brazilian mines, with improved results and widened range of conclusions that can be drawn related to bauxite processing.

1. Introduction

Bauxite is the main primary source for aluminium, accounting for around 44 Mt of metal produced from close to 220 Mt ore per year. Brazil holds the third position as bauxite supplier, accounting for 31 Mt in 2011, a market share of 14.1% (Bray, 2012a,b).

Bauxites are mostly products of very intense weathering of a broad spectrum of rocks, usually under hydrologic conditions of high percolation rates leaching out most of the elements, and enriching residual Al, Fe and Ti, as well as some other minor and trace elements (Costa, 1997). Being of supergene origin, bauxites are constituted by hydrated minerals, usually of low crystallinity, small crystal size and without distinctive optical properties. The mineralogical assemblage depends to some extend on the parent rocks, and on the geochemical evolution of the weathering profiles. Brazilian bauxites usually contain gibbsite, kaolinite, quartz, hematite, goethite and anatase as the main mineral phases.

Mineral processing of bauxites strongly depends on the mineralogical composition and the texture of the rock, a crucial factor for efficient hydrometallurgical Al extraction (Solymar et al., 2005). The aluminium carrier defines the necessary pressure, temperature and reagent concentration of the Bayer process for chemically leaching the element, while the silica carriers govern the digestion conditions (Authier-Martin et al., 2001). The settling rate of the red mud is particularly affected by the iron minerals, being higher when hematite dominates, and negatively impaired if cryptocrystalline phases are detected (Li and Rutherford, 1996). The increase of Al replacing Fe in the goethite and hematite structures significantly lowers the crystal size of the minerals (Cornell and Schwertmann, 2003), and are likely to be accounted for as the mentioned cryptocrystalline phases. Besides allowing the control over the deportment of aluminium to the sodium aluminate-rich liquor, or the red mud either as the insoluble goethite and hematite or the precipitated Bayer-sodalite, the fine mineralogical analysis also might help to predict the settling behaviour of the red mud.

Routine methods for ore characterisation, as ore microscopy, can usually not be applied to bauxite. Process control and performance prediction has therefore to rely on bulk methods, as chemical analysis and X-ray diffraction. More detailed studies may also include Mössbauer spectrometry to specifically assess the iron carriers (Kirwan et al., 2009), but is to some extend limited as the effect of Al-substitution and small crystal sizes on the hyperfine parameters of goethite is similar (Murad, 2010). X-ray diffraction remains as the most powerful tool to assess the mineralogy of bauxites.

* Corresponding author. Tel.: +55 21 3865 7263.
E-mail addresses: rneumann@cetem.gov.br (R. Neumann), angela.avelar@vale.com (A.N. Avelar), magela@iceb.ufop.br (G.M. da Costa).

0892-6875/$ - see front matter © 2013 Elsevier Ltd. All rights reserved.
http://dx.doi.org/10.1016/j.mineng.2013.09.020

In substitutional mixed crystals, lattice and site occupancy parameters are correlated, and both can be refined simultaneously by the Rietveld method, improving the mineral phase quantification and the overall refinement quality, due to the differences in the scattering coefficients of Fe and Al. Knorr and Neumann (2012) implemented the method for goethite, based on the displacement of the b lattice parameter as formulated by Schulze (1984). In several bauxite deposits, however, hematite is the main iron oxide, and is also prone to Al substitution. Here we present the implementation of the simultaneous refinement of the Al-for-Fe and OH^--for-O^{2-} substitution in hematite, based on the experimental work of Stanjek and Schwertmann (1992) for bauxite.

2. Materials and methods

2.1. Materials

Two sets of bauxite samples were studied. For the comparison of iron deportment with the results of Mössbauer spectroscopy, a first set of ten samples from the Trombetas (Mineração Rio do Norte – MRN) and Paragominas (Mineração de Bauxita Paragominas – MBP) mines from northern Brazil, as well as from the Kibi deposit in Ghana, were analysed (Avelar, 2011).

The same refining strategy was then applied to eleven Certified Reference Materials (CRM) available from CETEM (http://www.cetem.gov.br/pmrc-en.php), which had already been evaluated by the Rietveld method for the Al-for-Fe substitution (Knorr and Neumann, 2012).

2.2. Methods

Representative samples (around 5 g) were ground for 10 min in 12 mL of ethanol in a McCrone Micronizing Mill with agate grinding media. This is accepted as the standard procedure, avoiding damage to the crystal structures while effectively reducing particle size to below 10 μm (Dermatas et al., 2007; Kleeberg et al., 2008). Samples were discharged into PTFE Petri dished and dried at 343 K, under air flow. After drying the samples were gently ground with agate mortar and pestle, and backloaded into sample holders for X-ray diffraction analysis.

X-ray diffraction analysis was performed on a Bruker-AXS D4 Endeavor diffractometer, with Co kα radiation, Fe kβ filter and a LynxEye position sensitive detector (PSD). Diffraction patterns were acquired from 4 to 105° (2θ) at 0.02° steps, counting time of 1 s per step, resulting in accumulated 183 s per step due to the PSD. The identification of all the minerals was done with Bruker-AXS's DIFFRAC.EVA suite and PDF4 + 2012 relational database (ICDD, 2012).

Rietveld method-based mineral quantification with a fundamental parameters approach (Cheary and Coelho, 1992) was performed with the help of Bruker-AXS's Topas 4.2 software. Crystal structure information for the minerals was supplied by the Bruker Structure Database. Refining was performed considering seven diffraction lines for kα and one for kβ, as the Fe filter does not remove all kβ radiation. Background was calculated by a fifth order polynomial, and Lorentz polarization was fixed at zero.

For most minerals, only the lattice parameters, the scale factors and the Lorentzian contribution to crystal size were allowed to be refined. After careful analysis of several bauxite samples under the SEM, two generations of gibbsite and goethite were established, and the crystal size parameter was adjusted to allow for refinement of both without excessive correlation. Gibbsite was divided into coarse (50–10000 nm) and fine (>10 nm) fractions, and for the coarse fraction the Gaussian contribution to crystal size was also allowed to refine, to account for textural effects. Goethite was also split into coarse (same range as coarse gibbsite) and fine fractions. Fine goethite was restricted to 30–100 nm, and the isomorphous Al-for-Fe substitution calculated following Knorr and Neumann (2012).

The correlation of lattice parameters and site occupancy is not as straightforward for hematite as it is for goethite. As Stanjek and Schwertmann (1992) pointed out, the Al-for-Fe substitution in hematite deviates considerably from the Vegard line connecting the cell-edge lengths of hematite and corundum, due to a coupled OH^--for-O^{2-} substitution. The authors therefore postulate a more precise and unambiguous formula for hematite, $(Fe_{1-x}Al_x)_{2-z/3}(OH)_zO_{3-z}$. The OH^--for-O^{2-} substitution was analysed as water by weight loss (or loss on ignition, LOI), and the equations below correlate lattice parameters a and c, as well as the cell volume V, to the Al (mol%) and LOI (mass%):

$$a = 5.0359 - 0.00183\mathrm{Al} + 0.00175\mathrm{LOI} \quad (1)$$

$$c = 13.740 - 0.00512\mathrm{Al} + 0.0130\mathrm{LOI} \quad (2)$$

$$V = 301.78 - 0.330\mathrm{Al} + 0.493\mathrm{LOI} \quad (3)$$

The hydroxyl-for-oxygen substitution mostly affects the c parameter in hematite, and Stanjek and Schwertmann (1992) found the relation of the shift in the c parameter (compared to water-free hematite) to the loss on ignition

$$\Delta c = 0.008411 + 0.01305\mathrm{LOI} \quad (4)$$

to be highly significant ($r = 0.933$). From the hematite formula $(Fe_{1-x}Al_x)_{2-z/3}(OH)_zO_{3-z}$, it was graphically calculated (Fig. 1) that, for z up to 0.44, LOI = $18.561X_{OH^-}$ (X_{OH^-} in molar fraction), considering the coupled substitution $z = 2.2x$ as averaged by Stanjek and Schwertmann (1992).

As the c parameter of a hematite without substitutions equals 13.7454 Å, the hydroxyl-for-oxygen substitution can thus be refined following Eq. (5):

$$X_{OH^-} = (c - 13.7454)/0.24222 \quad (5)$$

The occupancy of aluminium in the iron site of the hematite structure, however, affects both the lattice parameters a and c, and was derived from Eqs. (1) and (3) as:

$$X_{Al} = (6019.83338 - 1518.37137 * a + 4.66753 * a^2 * c)/100 \quad (6)$$

Both occupancies are already in mol fraction. The sum of the hydroxyl-for-oxygen substitution occupancy is forced to 1 ($X_{OH^-} + X_{O^{2-}} = 1$), but the charge imbalance due to this substitution has to be compensated by a vacancy in the Fe(Al) sites, therefore $X_{Al} + X_{Fe} \leqslant 1$. The hematite formula $(Fe_{1-x}Al_x)_{2-z/3}(OH)_zO_{3-z}$

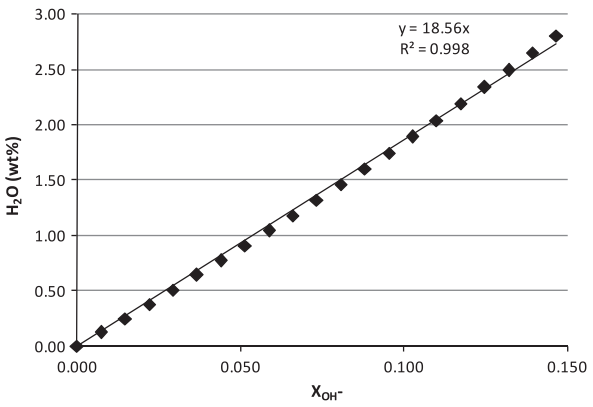

Fig. 1. Graphical calculation of the LOI (H_2O wt%) and X_{OH^-} (molar fraction) correlation.

states that each O^{2-} atom substituted by an OH^- requires ⅓ Fe (or Al) positions to be vacant, thus $X_{Al} + X_{Fe} = (1-⅓\ X_{OH^-})$, and the iron remaining in the site might be written as:

$$X_{Fe} = (1 - (c - 13.7454)/0.72666) - (6019.83338 - 1518.37137 * a + 4.66753 * a^2 * c)/100 \quad (7)$$

Eqs. (5)–(7) were implemented in the TOPAS graphical user interface. As all equations relate to the c parameter, tight constrains are necessary for both parameters, which were allowed to vary $5.010 \geqslant a \geqslant 5.039$ and $13.7454 \geqslant c \geqslant 13.8544$.

All samples were also analysed for its chemical composition, loss on ignition (LOI) and the Bayer process-related parameters total available alumina (TAA) and reactive silica ($r{\cdot}SiO_2$). TAA and $r{\cdot}SiO_2$ are measured after hydroxide digestion of the samples, and represent the soluble part of the oxides under *P* and *T* conditions that reproduce the Bayer process in laboratory. For the CRM's, these are certified values.

The first set of samples was also analysed by Mössbauer spectrometry at room temperature and at 77 K, using a $^{57}Co/Rh$ source, 1024 channel analyser, and α-Fe as calibration standard. Samples were mixed with glucose to adjust concentration. Spectra were fitted to Lorentzian curves with the MOSF software, or to a hyperfine magnetic field- and/or quadruple splitting-independent model by the DIST3E software (Vandenberghe, 1991). The relative areas of the doublets/sextets are proportional to the amount of each iron-bearing phase. The weight% of each component is calculated using these relative areas and the total iron content as determined by chemical analysis.

3. Results and discussion

Table 1 presents the mineralogy of the first set of samples, as well as the substitutions in goethite and hematite refined by the proposed Rietveld method calculation. For hematite, the overall Fe(Al) site occupancy, the charge balance and the relation of the OH^-/Al substitutions are also presented.

Goethite is highly substituted, close or at the maximum determined value of 36% (mol) in natural samples (Schwertmann and Carlson, 1994). This high value for the Al-substitution seems to be reasonable due to the extremely aluminium-rich environment.

The aluminium content in hematite, on the other hand, ranges between 5.7 and 12.2 mol%, while the OH^- for O^{2-} substitution is between 4.3 and 9.2 mol%. The OH^-/Al ratio is thus well below the 2.2 averaged by Stanjek and Schwertmann (1992), and it might be reasonable to infer that the hematite crystals from bauxites lost some of the excess water over aging, compared to the recently synthesized samples used by the authors. As the $z = 2.2x$ relation was necessary to graphically define the LOI to X_{OH^-} correlation, and thus solve Eq. (4), it was repeated using the average OH^-/Al from Table 1, $x = z$. From the new correlation, $LOI = 18.18X_{OH^-}$, Eq. (5) can be replaced by

$$X_{OH^-} = (c - 13.7454)/0.23725 \quad (8)$$

The difference between both equations is minimal, and the new refinement of all the X-ray diffraction patterns from the first set of samples after implementation of Eq. (8) into the Topas GUI gives results almost identical to the ones presented in Table 1.

The room-temperature Mössbauer spectra of all ores are similar and basically show the same features: a relatively sharp sextet, a broad and asymmetrical sextet with low intensity, and a central doublet (Fig. 2, bottom). The derived hyperfine parameters indicates that the outer sextet is due to hematite, whereas the inner sextet is due do goethite with low/medium Al-for-Fe substitution (Vandenberghe et al., 2000). The doublet might be due to superparamagnetic (SP) goethite or hematite, a phenomenon that occurs for isomorphic substitutions above approximately 15 mol% or for particle sizes below 15–20 nm (Murad and Johnston, 1987). The superparamagnetic behaviour can be easily demonstrated by collecting the Mössbauer spectra at 77 K. An increase in the relative area of the sextet, or even the appearance of a new sextet with a relative area similar to the decrease shown by the area of the doublet, is a confirmation for the superparamagnetic character.

Indeed, it can be seen in Fig. 2 (top) that the area of the doublet has substantially decreased at 77 K. The visual identification of the sextet belonging to goethite in these low temperature spectra is a little more complicated by the fact that the hematite exhibits two sextets at this temperature and by the greater temperature dependence of the hyperfine field of goethite. Pure and well crystallized hematite is weakly ferromagnetic at 298 K, and transforms to an antiferromagnetic phase at 263 K (Murad and Johnston, 1987). This transformation is known as Morin transition, and occurs at lower temperatures as the amount of foreign ions in the structure of hematite increases or as the particle sizes decreases (Murad and Johnston, 1987). Thus, the existence of two hematite sextets in the 77 K spectra of the present samples indicates that the hematite existing in these bauxites contain aluminium in the structure and possess small crystallites sizes. The decrease in the relative area of

Table 1
Mineralogy and substitutions of the first set of samples, as calculated by XRD and the Rietveld method (wt%, molar fraction for the substitutions).

	MBP71	MBP72	MBP73	MBP74	MBP75	MRN76	MRN77	MRN78	MRN79	Ghana
Anatase	1.0	1.5	2.0	1.8	1.4	1.0	1.3	1.4	1.2	2.8
Kaolinite	12.0	14.2	23.2	18.9	18.0	6.0	3.3	5.0	6.7	4.7
Quartz	2.0	1.4	1.3	1.2	1.4	1.9	3.6	1.4	1.3	1.2
Gibbsite, fine	60.9	52.3	45.3	51.0	50.2	60.1	55.0	58.0	58.6	51.8
Gibbsite, coarse	12.6	12.0	9.7	9.7	15.0	25.8	27.7	19.3	22.4	4.7
Goethite, constrained	4.1	5.2	7.3	8.0	4.8	1.5	1.8	2.6	1.1	22.2
Goethite, coarse	1.5	1.6	2.6	1.3	1.8	0.9	2.2	1.3	0.9	8.4
Hematite, constrained	4.6	10.8	7.6	7.2	6.4	1.9	4.0	10.1	6.9	1.8
Zircon	1.1	1.0	1.1	0.9	1.0	0.8	1.0	0.9	0.9	0.7
Boehmite	0.0	0.0	0.0	0.0	0.0	0.0	0.0	0.0	0.0	1.0
Grossularia	0.0	0.0	0.0	0.0	0.0	0.0	0.0	0.0	0.0	0.7
Σ gibbsite	73.5	64.3	55.0	60.7	65.2	85.9	82.7	77.3	81.0	56.5
Σ goethite	5.7	6.8	9.9	9.2	6.6	2.5	4.0	3.9	1.9	30.6
X_{Al} goethite	0.311	0.360	0.345	0.360	0.360	0.360	0.360	0.360	0.360	0.313
X_{Al} hematite	0.081	0.066	0.057	0.063	0.057	0.067	0.058	0.072	0.087	0.122
X_{Fe} hematite	0.892	0.907	0.929	0.920	0.922	0.916	0.913	0.902	0.885	0.847
X_{OH^-} hematite	0.081	0.081	0.043	0.051	0.064	0.050	0.086	0.078	0.085	0.092
Vacancy at Fe(Al) site	0.027	0.027	0.014	0.017	0.021	0.017	0.029	0.026	0.028	0.031
Charge	0.1	0.1	0.0	0.1	0.1	0.0	0.1	0.1	0.1	0.1
OH^-/Al	1.0	1.2	0.8	0.8	1.1	0.7	1.5	1.1	1.0	0.8

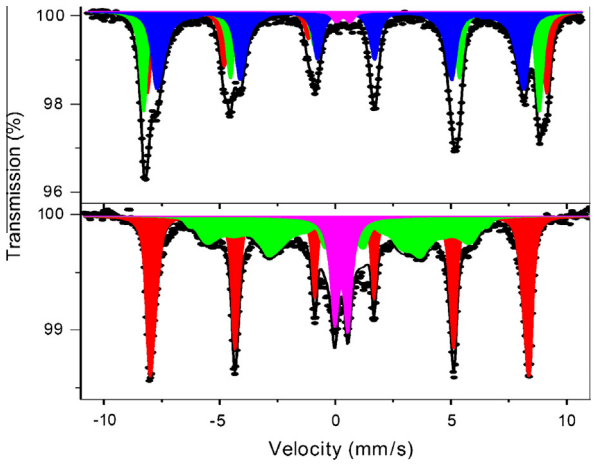

Fig. 2. Mössbauer spectra of sample MRN077 at room-temperature (bottom) and 77 K (top). Crosses represent the experimental data and the solid lines represent the adjusted sub spectra and their sum.

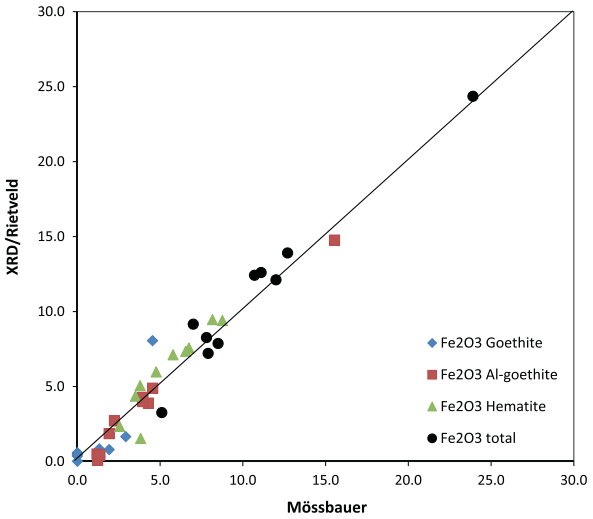

Fig. 3. Comparative graphs of Fe_2O_3 assigned to its carriers by XRD/Rietveld analysis and chemical assay/Mössbauer spectroscopy (wt%).

the doublet with $E_Q \sim 0.60$ mm/s was followed by an increase in the relative area of the sextet due to goethite. Thus, it is clear that the doublet seen in the 298 K spectrum, or at least the major part of it, is due to superparamagnetic goethite and not to superparamagnetic hematite.

The hyperfine magnetic fields indicate substitution below 11% for all MBP and MRN samples (de Grave et al., 1988), and substitutions between 4.1% and 7.7% using the low-temperature hyperfine fields (de Grave et al., 1982). If compared to room temperature data from Jonás et al. (1980), the substitutions are close no nil. There is no data at 77 K for the bauxite from Ghana, but the room-temperature hyperfine fields yield Al-for-Fe substitution close to 16% (de Grave et al., 1988), or 7–12% (de Grave et al., 1982), and 5% considering the work of Jonás et al. (1980).

Table 2 shows the chemical analysis results and iron distribution derived from the Mössbauer spectra for the first set of samples.

The iron oxide assigned to goethite, Al-goethite and Al-hematite as calculated by the Rietveld Method is compared to chemical assay/Mössbauer spectroscopy results in Fig. 3.

The comparison of the data shows a very good agreement between the Rietveld refined contents and those obtained by chemical analysis/Mössbauer data, although there is some deviation. Samples MBP72 to MBP75 might be slightly overground, thus affecting the quantification for hematite and goethite. Sample preparation was repeated for the other samples, with improvement of the results, but there was no sample left of those mentioned. The best-coinciding values are those related to Al-goethite.

The Rietveld method refines all the crystalline phases in the sample, and the slightly better matches for the iron by its carrying minerals, as presented above, is the result of a better refinement that affects the quantification of all minerals. Fig. 4 presents the comparison of the chemical assays to the elements derived from the XRD/Rietveld method-based phase quantification, respectively with no substitution refined, only in goethite, and for both goethite and hematite. TAA is compared to the alumina carried by gibbsite (gibbsite and boehmite for the sample from Ghana), and r·SiO_2 is compared to the kaolinite-carried silica.

Fig. 4 shows that the conciliation of chemical analysis and calculated chemistry improves when the substitutions are fitted. It has been suggested that some of the samples have been overground, and indeed it can be seen in Fig. 4 that samples 2–5 display the largest deviations from expected values. These possibly overground samples relate to the SiO_2 analyses that are out of the trend, overestimated by Rietveld phase quantification, and the kaolinite-bond reactive silica (r·SiO_2) seems actually to be responsible for most of the deviation. Kaolinite might be the most fragile mineral in bauxite, prone to have its structure damaged by grinding.

The results of phase quantification and of the substitutions in goethite and hematite of the Certified Reference material from CETEM are presented in Table 3. These are the same samples analysed by Knorr and Neumann (2012), although some refinement details differ, as using two generations of goethite instead of only one, besides hematite substitutions being fitted.

These samples also show Al-for-Fe substitutions in Al-goethite close or at the maximum allowed limit, as expected for goethite grown in an extremely Al-rich environment, together with the coarse and not-substituted goethite. The advantage of fitting two generations of goethite (and gibbsite) is that inherited minerals,

Table 2
Chemical assays of the first set of samples and Fe_2O_3 assigned to the iron carriers as measured by Mössbauer spectroscopy (wt%).

	MBP71	MBP72	MBP73	MBP74	MBP75	MRN76	MRN77	MRN78	MRN79	Ghana
Al_2O_3	54.2	54.8	53.9	53.9	57.9	57.8	56.2	53.1	55.8	42.1
SiO_2	8.4	3.5	5.4	4.4	4.3	3.9	3.9	2.9	3.6	2.2
Fe_2O_3	7.8	12.7	10.7	11.1	7.0	5.1	7.9	12.0	8.5	23.9
TiO_2	2.0	2.1	1.9	1.8	1.6	1.1	1.5	1.3	1.1	2.9
LOI	27.3	27.7	27.6	28.0	29.3	30.5	29.4	28.5	29.3	25.5
Total	99.7	100.8	99.5	99.2	100.1	98.4	98.9	97.8	98.3	96.6
TAA	46.6	50.0	48.5	48.8	53.3	56.8	54.8	51.1	51.1	37.6
r·SiO_2	6.7	2.8	4.5	3.7	3.4	3.2	1.7	2.5	3.1	1.3
Fe_2O_3 goethite	0.0	0.0	0.0	0.0	0.0	1.3	2.9	1.9	1.4	4.5
Fe_2O_3 Al-goethite	4.3	3.9	4.0	4.6	2.2	1.2	1.2	1.9	1.4	15.5
Fe_2O_3 hematite	3.5	8.8	6.7	6.5	4.8	2.6	3.8	8.2	5.8	3.8

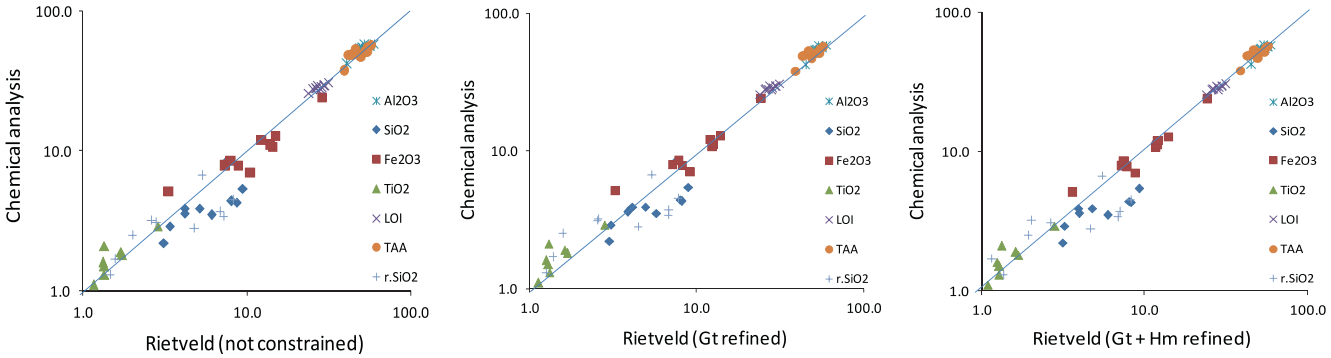

Fig. 4. Conciliation of chemical composition derived from XRD/Rietveld analysis against the chemical analysis (wt%).

Table 3
Mineralogy and substitutions of CETEM's Certified Reference Materials, as calculated by XRD/the Rietveld method (wt%, molar fraction for the substitutions).

	BXGO-1	BXMG-1	BXMG-2	BXMG-3	BXMG-4	BXMG-5	BXPA-1	BXPA-2	BXPA-3	BXPA-4	BXSP-1
Anatase	0.3	0.2	0.4	1.2	1.8	1.3	1.4	1.3	1.2	0.9	1.8
Kaolinite	0.3	4.3	6.9	2.3	13.0	15.9	7.2	9.2	6.9	6.8	13.0
Quartz	1.5	2.7	5.8	1.9	1.4	1.3	1.9	1.5	1.1	1.2	5.9
Gibbsite, fine	58.2	52.1	54.7	41.5	53.6	51.5	59.3	63.8	63.7	67.6	57.6
Gibbsite, coarse	32.7	11.9	13.1	6.2	6.7	7.6	14.2	12.8	11.4	13.9	3.1
Goethite, constrained	4.8	14.9	13.1	19.5	8.3	9.3	0.7	3.1	3.7	2.6	7.5
Goethite, coarse	0.3	2.9	2.6	5.0	1.0	0.9	2.7	1.7	1.4	0.9	0.4
Hematite, constrained	0.6	8.4	2.8	22.3	1.7	1.1	11.7	5.7	9.7	5.1	2.3
Zircon	1.2	0.8	0.5	0.2	1.0	1.0	0.9	0.9	0.8	1.0	1.0
Boehmite		1.8									
Muscovite					11.5	10.0					7.4
Σ gibbsite	90.9	64.0	67.9	47.7	60.3	59.1	73.5	76.6	75.1	81.5	60.7
Σ goethite	5.2	17.8	15.7	24.5	9.3	10.3	3.4	4.8	5.2	3.5	7.8
X_{Al} goethite	0.360	0.327	0.308	0.308	0.319	0.360	0.360	0.360	0.360	0.360	0.292
X_{Al} hematite	0.138	0.134	0.138	0.084	0.049	0.053	0.072	0.076	0.079	0.071	0.134
X_{Fe} hematite	0.816	0.716	0.712	0.897	0.914	0.908	0.884	0.905	0.893	0.893	0.808
X_{OH^-} hematite	0.141	0.459	0.459	0.057	0.114	0.121	0.136	0.057	0.085	0.112	0.178
Vacancy at Fe(Al) site	0.046	0.150	0.150	0.019	0.037	0.039	0.044	0.019	0.028	0.036	0.058
Charge	0.1	0.5	0.5	0.1	0.1	0.1	0.1	0.1	0.1	0.1	0.2
OH^-/Al	1.0	3.4	3.3	0.7	2.3	2.3	1.9	0.8	1.1	1.6	1.3

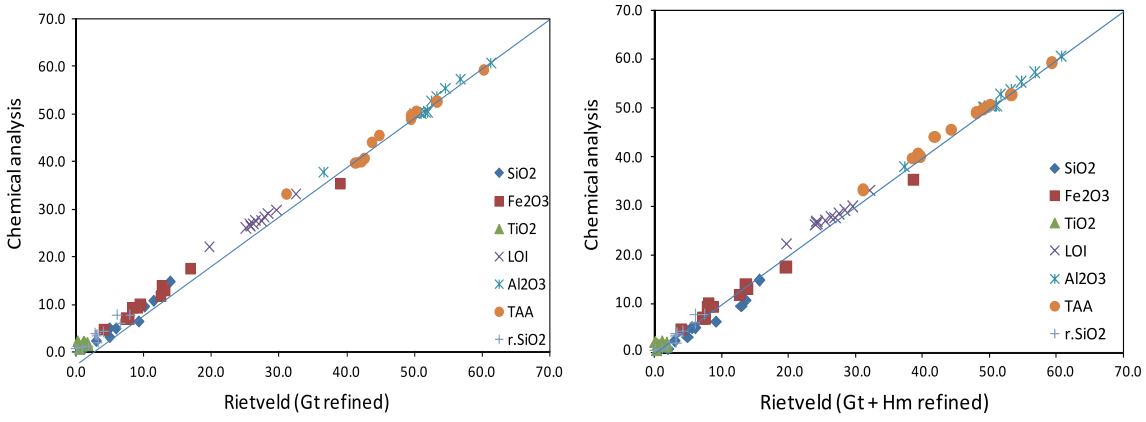

Fig. 5. Conciliation of chemical composition derived from XRD/Rietveld analysis and the chemical analysis of the CRMs (wt%).

or grown in an environment different than the present one, can be accounted for.

The Al substitutions in hematite range from 4.9% to 13.8% (mol), similar to what has been refined for the first group of samples. The OH^--to-O^{2-} substitutions range from 5.7% to 46%, being very high for two of the samples from Minas Gerais State (BXMG-1 and 2). The OH^-/Al ratio consequentially also varies much more for this sample set, from 0.7 up to 3.4. These results do not depend on the numerical solution chosen for the LOI to X_{OH^-} correlation, and employing Eq. (5) or (8) delivers quite the same result.

Only room-temperature Mössbauer spectra have been acquired for these samples, and hence it cannot be ensured that the entire doublet corresponds to high-Al, superparamagnetic goethite. As

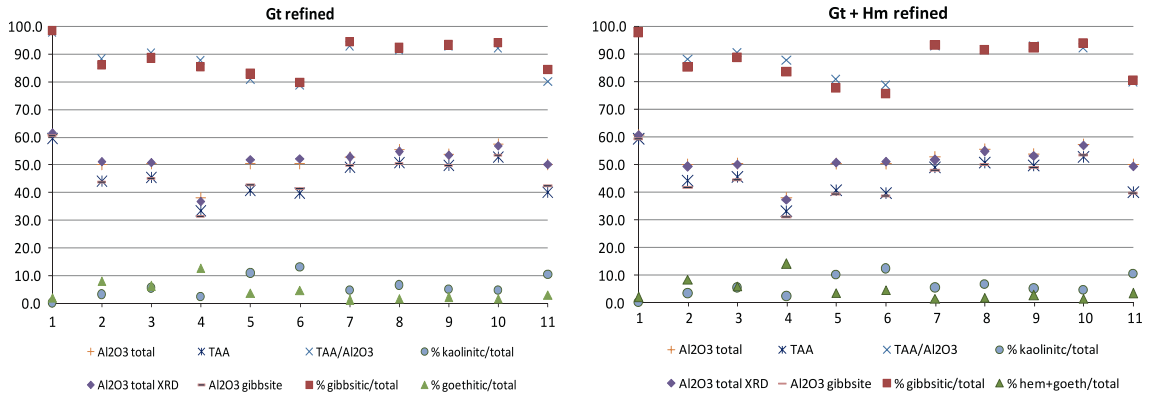

Fig. 6. Comparative graphs of chemical composition as assayed by chemical methods and derived from XRD/Rietveld mineralogical analysis of the CRMs (wt%).

far as Mössbauer data can be applied, however, XRD/Rietveld results are within the limits the spectroscopy imposes.

The conciliation of the chemical composition derived from the XRD data and Rietveld method against the certified chemical analysis is presented in Fig. 5, and in Fig. 6 the same data is compared as Bayer process-related variables. Both Figures compare results where only the substitution in goethite has been fitted, and where both, goethite and hematite, were refined.

The conciliation of Fig. 5 clearly indicates an overall improvement of the results when the substitutions in hematite are refined. The sample with the highest hematite content, BXMG-3, achieves a much better conciliation when the substitutions in hematite are considered, as expected. These results are also better than the previous ones obtained for the same samples (Knorr and Neumann, 2012) in which mixed crystals in goethite were already refined, although the improvement could be credited to the use of two generations of goethite.

Most important, however, are the results related to the Bayer process in Fig. 6, which cannot be assayed by other methods. Refining the substitutions in hematite, one can observe that the amount of alumina carried by gibbsite does not match TAA any more for some of the samples, possibly meaning that kaolinite might be releasing alumina at the TAA chemical analysis. Alumina from kaolinite, however, is not recovered in the hydrometallurgical process, as it precipitates as the sodium–aluminium silicate (Authier-Martin et al., 2001). The aluminium carried by the iron minerals is also not available for recovery, as these minerals are supposed to be inert to low-pressure digestion. When hematite is the dominant iron carrying species in the ore, as for the BXPA samples (7–10 in Fig. 6), the quantification of the aluminium bound to its lattice is paramount for mass balance.

4. Conclusions

The coupled Al-for-Fe and OH^{-}-for-O^{2-} isomorphous substitution in hematite, as modelled by Stanjek and Schwertmann (1992), was successfully implemented as a constrained refinement into the Rietveld method through the graphic interface of the Topas software, in addition to the Al-for-Fe substitution in goethite.

The method was tested with bauxite samples, and calculated results were in good agreement with direct ^{57}Fe Mössbauer spectroscopy measurements. The conciliation of chemical assays and the calculated chemical compositions as derived from quantitative phase analysis was also very good, and improved when the substitutions for both minerals – goethite and hematite, are fitted.

Sample preparation is of paramount importance, and overgrinding can induce significant errors into the phase quantification, as already pointed out, e.g., by Knorr and Bornefeld (2012).

The direct knowledge of the Al-carriers in bauxite is a powerful tool for process control, and provides mineralogical details complementary to the Bayer process-related parameters available alumina (TAA) and reactive silica (r·SiO_2). Working on a coupled chemical and mineralogical approach, the overall mass and metallurgical balance of the process is improved. By planning the feed of the Bayer process knowing the aluminium deportment, the prediction of the outcome can be optimized, and might even allow for better reagent dosage, as inert alumina can be excluded from the balance. Finally, a tool to measure Al substitution in iron minerals might correlate it to goethite and hematite crystal sizes, and thus to the settling behaviour of the red mud.

Acknowledgements

The authors thank VALE for allowing the results to be published. R. Neumann and G.M. da Costa acknowledge CNPq for research grants. The manuscript benefited from an anonymous reviewer's comments.

References

Authier-Martin, M., Forté, G., Ostap, S., See, J., 2001. The mineralogy of bauxite for producing smelter-grade alumina. JOM 53 (12), 36–40.
Avelar, A.N., 2011. Influência da mineralogia na etapa de separação da lama vermelha no processo Bayer,M.Sc. Dissertation, Escola de Minas da Universidade Federal de Ouro Preto, Ouro Preto, p. 112. <http://www.tede.ufop.br/tde_busca/arquivo.php?codArquivo=706>.
Bray, E.L., 2012a. Aluminum. In: Mineral Commodity Summaries. USGS, pp. 16–17.
Bray, E.L., 2012b. Bauxite and Alumina. In: Mineral Commodity Summaries. USGS, pp. 26–27.
Cheary, R.W., Coelho, A., 1992. A fundamental parameters approach to X-ray line-profile fitting. Journal of Applied Crystallography 25, 109–121.
Cornell, R.M., Schwertmann, U., 2003. The Iron Oxides: Structure, Properties, Reactions, Occurences and Uses. Wiley-VCH, Weinheim, p. 664.
da Costa M.L., Lateritization as a major process of ore deposit formation in the Amazon region, Exploration and Mining Geology 6 (1), 1997, 79-104.
de Grave, E., Bowen, L.H., Weed, S.B., 1982. Mössbauer study of aluminum-substituted hematites. Journal of Magnetism and Magnetic Materials 27 (1), 98–108.
de Grave, E., Bowen, L.H., Amarasiriwardena, D.D., 1988. ^{57}Fe Mössbauer effect study of highly substituted aluminum hematites: determintion of the magnetic hyperfine field substitutions. Journal of Magnetism and Magnetic Materials 72, 129–140.
Dermatas, D., Chrysochoou, M., Pardali, S., Grubb, D.G., 2007. Influence of X-Ray diffraction sample preparation on quantitative mineralogy. Journal of Environmental Quality 36 (2), 487–497.
ICDD, 2012. International Centre for Diffraction Data - PDF4+ Relational Powder Diffraction File, Newton Square, USA.
Jonás, K., Solymar, K., Zöldi, J., 1980. Some applications of Mössbauer spectroscopy for the quantitative analysis of minerals and mineral textures. Journal of Molecular Structure 60, 449–452.
Kirwan, L.J., Deeney, F.A., Croke, G.M., Hodnett, K., 2009. Characterisation of various Jamaican bauxite ores by quantitative Rietveld X-ray powder diffraction and ^{57}Fe Mössbauer spectroscopy. International Journal of Mineral Processing 91 (1–2), 14–18.

Kleeberg, R., Monecke, T., Hillier, S., 2008. Preferred orientation of mineral grains in sample mounts for quantitative XRD measurements: how random are powder samples? Clays and Clay Minerals 56 (4), 404–415.

Knorr, K., Bornefeld, M., 2012. Analysis of Iron Ore – A combined XRD, XRF and MLA study. In: Wills, B.A. (Ed.), Process Mineralogy '12. MEI – Minerals Engineering International, Cape Town, South Africa.

Knorr, K., Neumann, R., 2012. Advances in Quantitative X-Ray Mineralogy: Mixed Crystals in Bauxite. In: Broekmans, M.A.T.M. (Ed.), Proceedings of the 10th International Congress for Applied Mineralogy (ICAM). Springer, Berlin Heidelberg, pp. 377–384.

Li, L.Y., Rutherford, G.K., 1996. Effect of bauxite properties on the settling of red mud. International Journal of Mineral Processing 48 (3–4), 169–182.

Murad, E., Johnston, H.J., 1987. Iron Oxides and Oxyhydroxides. In: Long, G.I. (Ed.), Mössbauer Spectroscopy Applied to Inorganic Chemistry. Spring Street, New York, pp. 507–582.

Murad, E., 2010. Mossbauer spectroscopy of clays, soils and their mineral constituents. Clay Minerals 45 (4), 413–430.

Schulze, D.G., 1984. The influence of aluminum on iron oxides. VIII. Unit-cell dimensions of Al-substituted goethites and estimation of Al from them. Clays and Clay Minerals 32 (1), 36–44.

Schwertmann, U., Carlson, L., 1994. Aluminum influence on iron oxides: XVII. Unit-Cell parameters and aluminum substitution of natural goethites. Soil Science Society of America Journal 58, 256–261.

Solymar, K., Madai, F., Papanastassiou, D., 2005. Effect of Bauxite Microstructure on Beneficiation and Processing. In: Kvande, H. (Ed.), Light Metals. TMS, pp. 47–52.

Stanjek, H., Schwertmann, U., 1992. The influence of aluminum on iron oxides; Part XVI, Hydroxyl and aluminum substitution in synthetic hematites. Clays and Clay Minerals 40 (3), 347–354.

Vandenberghe, R., Barrero, C.A., Costa, G.M.D., van San, E., de Grave, E., 2000. Mössbauer characterization of iron oxides and (oxy) hydroxides: the present state of the art. Hyperfine Interactions 126, 247–259.

Vandenberghe, R., 1991. Mössbauer Spectroscopy and Applications in Geology, 2nd edn. Gent, Belgium.